Check for updates

View Article Online
View Journal

Journal of
Materials Chemistry A

Accepted Manuscript

This article can be cited before page numbers have been issued, to do this please use: L. Lin, K. Yang, R. Tan, M. Li, S. Fu, T. Liu, H. Chen and F. Pan, *J. Mater. Chem. A*, 2017, DOI: 10.1039/C7TA05469F.

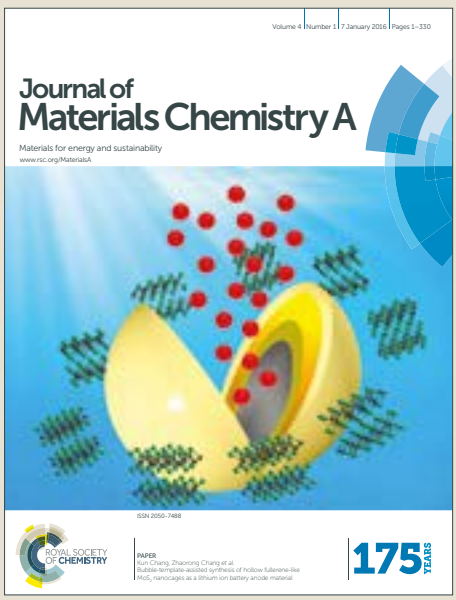

This is an Accepted Manuscript, which has been through the Royal Society of Chemistry peer review process and has been accepted for publication.

Accepted Manuscripts are published online shortly after acceptance, before technical editing, formatting and proof reading. Using this free service, authors can make their results available to the community, in citable form, before we publish the edited article. We will replace this Accepted Manuscript with the edited and formatted Advance Article as soon as it is available.

You can find more information about Accepted Manuscripts in the author guidelines.

Please note that technical editing may introduce minor changes to the text and/or graphics, which may alter content. The journal's standard Terms & Conditions and the ethical guidelines, outlined in our author and reviewer resource centre, still apply. In no event shall the Royal Society of Chemistry be held responsible for any errors or omissions in this Accepted Manuscript or any consequences arising from the use of any information it contains.

ROYAL SOCIETY OF CHEMISTRY

rsc.li/materials-a

View Article Online
DOI: 10.1039/C7TA05469F

Journal Name

ARTICLE

Published on 29 August 2017. Downloaded by University Town Library of Shenzhen on 30/08/2017 02:18:08.

Journal of Materials Chemistry A Accepted Manuscript

Effect of sulfur-containing additives on the formation of solid-electrolyte interphase evaluated by in-situ AFM and ex-situ characterizations†

Received 00th January 20xx,
Accepted 00th January 20xx

DOI: 10.1039/x0xx00000x

www.rsc.org/

Lingpiao Lin‡, Kai Yang‡, Rui Tan, Maofan Li, Shaojie Fu, Tongchao Liu, Haibiao Chen*and Feng Pan*

An effective solid-electrolyte interphase (SEI) layer is the key to the stable operation of lithium-ion batteries by minimizing loss of lithium and decomposition of electrolyte. Surfur-containing additives can facilitate the formation of SEI layers and the effect of two sulfur-containing additives was investigated in this work. The growth of the SEI layer on a highly oriented pyrolytic graphite substrate during a cyclic voltammetry scan was monitored *in-situ* using an atomic force microscope for imaging and the electrochemical workstation for controling the potential of the electrode simultaneously. Both ethylene sulfite (ES) additive and prop-1-ene-1,3-sultone (PES) additive can promote the formation of SEI layer at higher potentials. The ES additive started to form SEI at a higher voltage than the PES additive and the surface of the SEI layer appeared to be smoother. The effect of the additives was further evaluted in coin cells and the ES additive was found to enable superior stability of the cell in comparision to the PES additive and the neat electrolyte. Examination of the multi-cycled graphite electrode discovered that the SEI layer formed with the ES additive was thicker and denser with low resisitance for Li-ion conduction, which explains the high performance of the coin cell.

Introduction

With the rapid development of the clean energy industry, lithium ion batteries (LIBs) are becoming an important technology for electric energy storage owing to their high energy density and stable cycling performance. Electrolyte is a key element in an LIB and it can largely determine the performance of the battery. For years, researchers have continuously worked on optimizing the electrolyte to improve the performance of LIBs. One approach to enhance the performance of the battery is to tune the properties of the electrolyte by including various additives. Sulfur-containing compounds are selected for forming a stable solid-electrolyte interphase (SEI) layer as they are easier to be reduced than other components in the electrolyte.[1-4] Ethylene sulfite (ES) is one of the most commonly used additives. Since the early days, ES has been added in the $LiClO_4$ solution in LIBs with graphite anodes.[5] Adding ES in ethylene carbonate (EC) based electrolytes can noticeably improve the cycling performance at 0.2 C charge/discharge rate.[6] Wang et al. showed that ES can facilitate the growth of SEI on the surface of spinel lithium titanate (LTO) as the reduction potential was intentionally lowered to zero.[7] Researchers also investigated the role of ES in NMC($LiNi_{1/3}Mn_{1/3}Co_{1/3}O_2$)/graphite pouch cells using gas chromatography–mass spectrometry (GC-MS) and X-ray photoelectron spectroscopy (XPS), and they found that ES can form an effective SEI on the surface of graphite but not on the surface of NMC.[8] Recently, prop-1-ene-1,3-sultone (PES) as another sulfur-containing additive has also become interesting to the researchers. PES has been regarded to improve the performance of a LIB more significantly than propane sultone (PS) by facilitating the formation of an SEI layer on the surface of the graphite anode.[9] Accordingly, PES can help to form an SEI layer to effectively protect the graphite anode in propylene carbonate-based electrolytes.[10] For $LiNi_{1/3}Mn_{1/3}Co_{1/3}O_2$/graphite pouch cells, PES showed a similar effect as vinylene carbonate (VC) but demonstrated better stability at elevated temperatures.[11] Self et al. used density functional theory (DFT) to study the reaction of PES to form an SEI layer during charging and discharging in LIBs.[12] These previous studies on the effect of ES and PES additives were conducted using *ex-situ* characterization tools such as GC-MS, XPS, and SEM, and few researchers were able to investigate how these additives influence the initial formation of an SEI layer using *in-situ* technologies. In recent years, *in-situ* atomic force microscope (AFM) is becoming a powerful tool for visualizing the evolution of the surface of the electrodes in LIBs during electrochemical processes,[13-26] especially for investigating the evolution of the SEI layer on the graphite electrode.[16, 21-24, 27, 28] The *in-situ* AFM can be operated simultaneously with electrochemical control which can well

School of Advanced Materials, Peking University, Shenzhen Graduate School, Shenzhen 518055, People's Republic of China
**E-mail: chenhb@pkusz.edu.cn; panfeng@pkusz.edu.cn*
† Electronic Supplementary Information (ESI) available: Additional characterization data. See DOI: 10.1039/x0xx00000x
‡ These authors contributed equally to this work.

Please do not adjust margins

View Article Online
DOI: 10.1039/C7TA05469F

Published on 29 August 2017. Downloaded by University Town Library of Shenzhen on 30/08/2017 02:18:08.

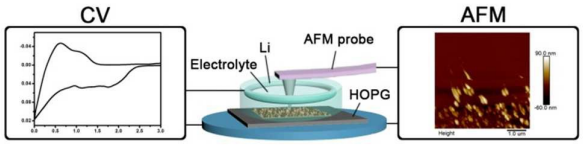

Fig. 1 Schematic of *in-situ* AFM cell configuration for measuring CV and surface morphology simultaneously. The cell is connected with electrochemical workstation and AFM imaging control system.

simulate the process in a real device with minimal interference.

The effect of ES or PES additive in the $LiPF_6$ EC/DMC electrolyte on the initial formation of the SEI layer in LIBs has not been observed directly, and how these additives affect the performance of LIBs at high charge-discharge rates has not been investigated. In this work, we visualized the evolution of the SEI layer on the fresh surface of the graphite anode by using an *in-situ* AFM coupled with an electrochemical workstation for collecting morphological images under simultaneous potential control and current measurement, and identify subtle difference between the effects of ES and PES on the formation of the SEI layer on the graphite anode. The effect of ES and PES on the performance of the batteries was verified by testing graphite/Li-metal half-cells at various charge-discharge rates. Subsequently, high resolution transmission electron microscope (HRTEM) was used to evaluate the quality of the SEI layers formed without any additive, with ES additive, and with PES additive.

Experimental

As shown in Fig. 1, the *in-situ* AFM cell was composed of a piece of highly oriented pyrolytic graphite (HOPG) substrate ($12 \times 12 \times 2$ mm^3, ZYB Grade, Bruker Corporation), electrolyte, a lithium ring and an AFM scanning probe. The HOPG substrate was situated at the bottom of the AFM fluid cell (MMTMEC type) and the lithium ring was mounted inside the cell groove (Fig. S1). The HOPG substrate was cleaved with adhesive tape to expose a fresh surface and used as the working electrode (Fig. S2), and the lithium ring was used as the counter and the reference electrode. Electrolyte with 1.0 M $LiPF_6$ in ethylene carbonate/dimethyl carbonate solution (EC/DMC, volume ratio of 1:1) and 1 wt% additive was injected into the cell. Both electrodes were connected to a CH1030C electrochemical workstation (Chenhua Instrument Co., Ltd., China) for cyclic voltammetry (CV) measurements. The cell was mounted into an AFM system (Bruker Multimode 8 with a Nanoscope V controller) for imaging and the electrochemical workstation was used to control the potential of the electrode simultaneously. The whole *in-situ* experiment was conducted in an argon-filled glovebox (MIKOUNA, $H_2O \leq 0.1$ ppm, $O_2 \leq 0.1$ ppm) at room temperature. AFM topography was collected in Fluid-Scanasyst mode simultaneously with at a scanning rate of 2 mV s^{-1} between 3.0 and 0 V.

The effect of the additive on the performance of the LIBs was evaluated in type CR2032 coin cells. The graphite electrode was prepared by mixing graphite powders (BTR New Energy Technology Co., Ltd, China, see Fig. S13 for SEM), acetylene black, and polytetrafluoroethylene (PTFE) binder in a ratio of 7:2:1. Same 1.0 M $LiPF_6$ in EC/DMC solution with 1 wt% additive was used as the electrolyte (60 μL per cell) and a lithium pellet was used as the counter electrode. The coin cells were assembled in an argon-filled glovebox, and transferred to a thermostatic oven for electrochemical tests. The coin cells were rested at 25 °C for one day before the tests. Charging-discharging tests were conducted on a LAND-CT2001A battery testing system (Rambo Testing Equipment Co., Ltd., China).

After charging-discharging for 50 cycles at 5 C rate, the coin cells were disassembled and the graphite electrode was removed for further analysis. SEM images of the surface of the electrode were acquired using a Zeiss Supra 55 SEM. The elemental and chemical state of the surface was analysed using XPS on an ESCALAB 250XL spectrometer. The cross-section of the electrode was prepared using focused ion beam (FIB, FEI Scios). The preparation workflow is shown in Fig. 2. A relatively flat region was selected and a 1 μm thick Pt layer was deposited to protect the surface of the SEI layer. A Ga ion beam was employed to cut out a vertical slice in the selected area. The slice was then transferred to a special "U" style copper holder and was further thinned down to ~20 nm by ion milling with controlled Ga ion beam. TEM images of the cross-section were acquired using an FEI Tecnai G2 F30 microscope.

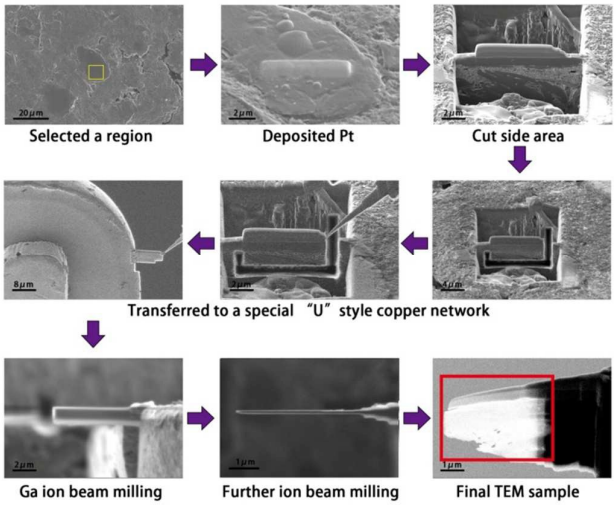

Fig. 2 Preparation of the cross-section of the SEI layer using FIB.

Results and discussion

Effect of additive on the formation of SEI on fresh graphite surface

Fig. 3 shows the CV and corresponding *in-situ* AFM results for a regular 1.0 M $LiPF_6$/EC/DMC electrolyte without additive, with 1% ES and with 1% PES. The results for the regular electrolyte are shown in Figs. 3, S3 and S4, and they agree well with previous studies. As the blue CV curve shows, before the voltage reached 1 V during the cathodic sweeping, there were several small steps in current. However, the surface of the HOPG remained clean with the characteristic atomically smooth structure as shown by the AFM images. The current in

Journal of Materials Chemistry A Accepted Manuscript

This journal is © The Royal Society of Chemistry 20xx

Please do not adjust margins

View Article Online
DOI: 10.1039/C7TA05469F

Published on 29 August 2017. Downloaded by University Town Library of Shenzhen on 30/08/2017 02:18:08.

this region is believed to originate from the reduction of oxygen or other contaminants dissolved in the solution, and it was not associated with the formation of any solid phases.[21, 25, 27] The first evident cathodic peak appeared at around 0.7 V, and it can be attributed to the onset of SEI growing on the HOPG substrate as particles started to appear in the AFM image at the corresponding potential.[29] Apparently, *in-situ* AFM observation provided unique information for identifying at what potential precipitates started to form on the surface during CV scanning.

The cathodic CV scanning in the ES-containing electrolyte is shown as the magenta curve in Fig. 3. Similarly, although the CV current began to increase at 2.4 V, there was no obvious change to the basal plane as the AFM image shows. The magnitude of the current started to increase as the potential was lowered to about 2.40 V and the current reached a peak at a potential around 1.75 V. In the AFM images, several particles started to appear at around 1.86 V and many more particles appeared at 1.70 V, which can be related to the first current peak at around 1.75 V. The height profile (Fig. S6) reveals that the height of these initial particles was in the range of 40-60 nm and the lateral dimension of the particles

Fig. 3 Cathodic CV curves of the freshly cleaved HOPG electrode in 1.0 M $LiPF_6$/EC/DMC with no additive, 1% ES and 1% PES at a scan rate of 2 mV s^{-1}, and corresponding *in-situ* AFM images showing the evolution of the surface of HOPG. The arrow indicates the scan direction of both CV and AFM. The AFM images were rotated 90 degrees to match voltage scale of the CV.

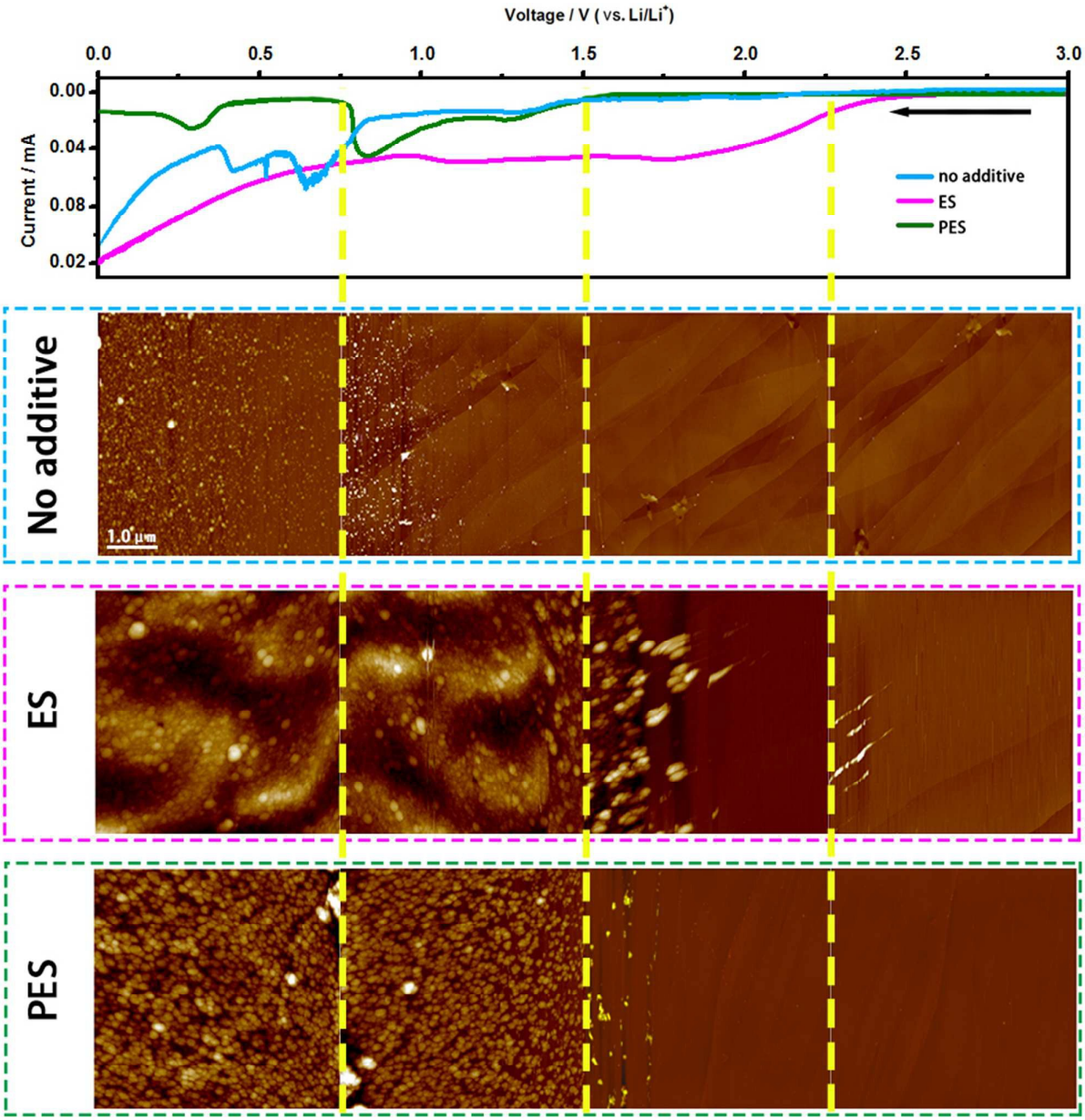

Journal of Materials Chemistry A Accepted Manuscript

Please do not adjust margins

View Article Online
DOI: 10.1039/C7TA05469F

Published on 29 August 2017. Downloaded by University Town Library of Shenzhen on 30/08/2017 02:18:08.

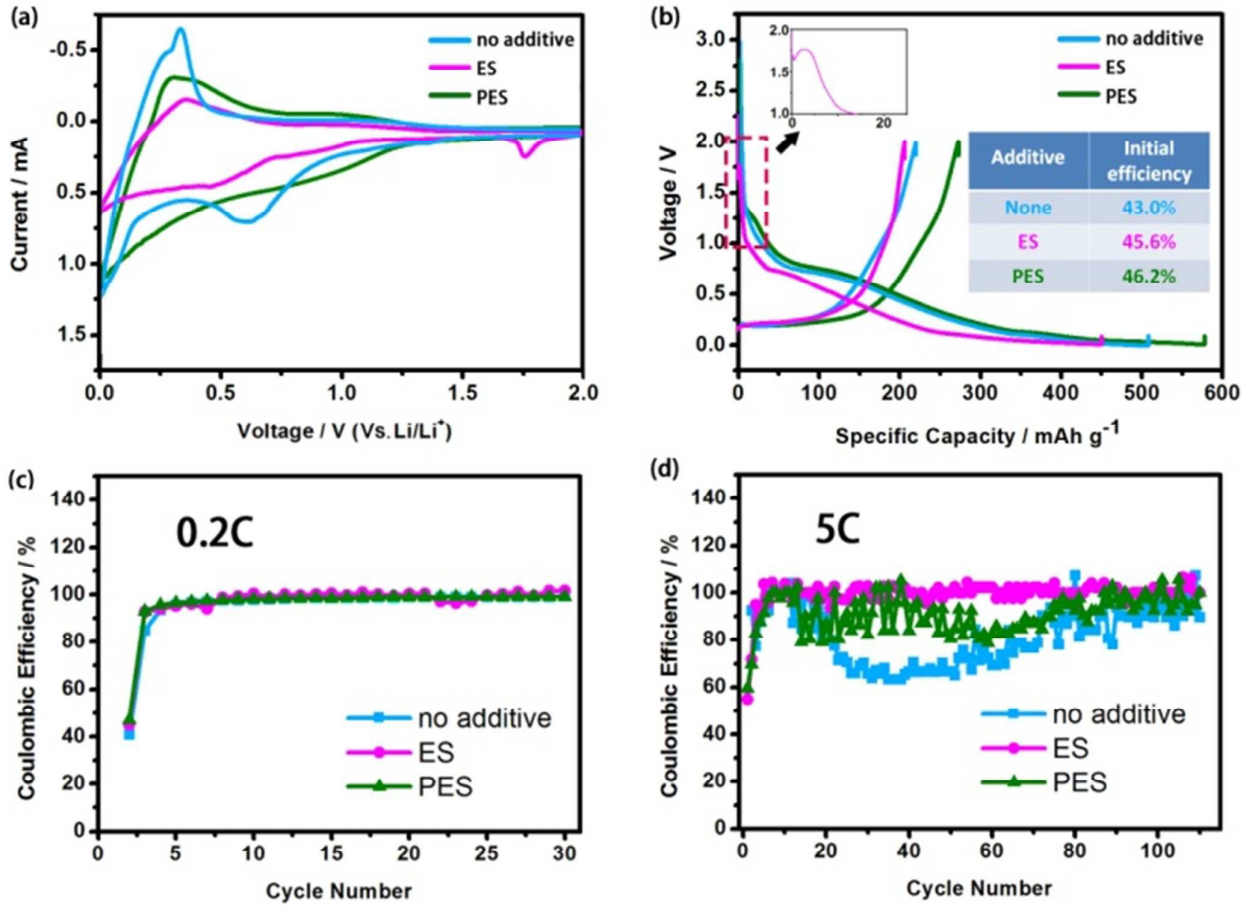

Fig. 4 (a) CV scanning of fresh coin cells with and without additives in 1.0 M $LiPF_6$/EC/DMC electrolyte. (b) The first charge-discharge curve and initial efficiency of the coin cells with three types of electrolytes at 0.5 C rate. The cycling stability of coin cells with three different types of electrolytes at (c) 0.2 C rate and (d) 5 C rate as expressed in the coulombic efficiency as a function of cycle number. All coin cells were activated at 0.2 C for two cycles prior to cycling.

was about 500 nm. We can infer that the observed particles were the product of the reduction of ES, which took place at a potential much higher than that in the electrolyte without any additives.[6] From 1.60 V to 1.13 V, the magnitude of the current slowly increased and reached the second peak at 1.13V. Afterwards, the magnitude of the current increased sharply from 0.80 V to 0 V, which is attributed to the lithium intercalation process. Further decrease of the potential induced reduction of ES to form insoluble precipitates covering the whole surface of the HOPG substrate, which remained essentially unchanged from 0.78 V to 0 V. As the potential increased from 0 V to 0.60 V, the trend of the current reversed and the anodic current reached a peak at around 0.60 V, signifying the lithium deintercalation process (Fig. S5). The surface of the HOPG remained unchanged during the whole anodic sweeping (Fig. S5) and the morphology remained unchanged during the second and the third sweeping cycles (Fig. S7). Quasi-static AFM tests were carried out to reveal how SEI evolves if the electrode is held at some critical potentials. When the potential was held above the reduction potential of ES, very little SEI formed (Fig. S8). SEI gradually covered the whole HOPG surface when the potential was decreased to bellow the reduction potential of ES. The surface remained unchanged once the SEI covered the whole HOPG surface (Fig. S9).

The CV scanning in the PES-containing electrolyte is shown as the green curve in Fig. 3. The cathodic current was negligible before the potential was lowered to 1.6 V. At 1.6 V, the reduction reaction of PES started as signified by the increase in the magnitude of the current and the appearance of several particles as observed by AFM. Therefore, PES also has a higher reduction potential in comparison to the regular electrolyte. Previously reported reduction potential of PES was around 1.3 V,[12] still lower compared to that of ES. There are two peaks at 1.3 V and 0.7 V within the broad reduction potential range. In this potential region, more particles formed and gradually covered the whole HOPG surface as visible in AFM images. The height profile (Fig. S11) shows that the height of the initial particles is in the range of 10-40 nm and the lateral dimension of the particle is in the range of 100-300 nm. Both the thickness and the lateral dimension of the precipitates from PES are smaller than those of the precipitates from ES. As the potential sweeping continues, there is a weak lithium intercalation peak at around 0.3 V, which is notably different from the CV of the ES-containing electrolyte. Similarly, a weak peak appears at 0.72 V with the anodic sweeping and it

Journal of Materials Chemistry A Accepted Manuscript

This journal is © The Royal Society of Chemistry 20xx

Please do not adjust margins

View Article Online
DOI: 10.1039/C7TA05469F

Published on 29 August 2017. Downloaded by University Town Library of Shenzhen on 30/08/2017 02:18:08.

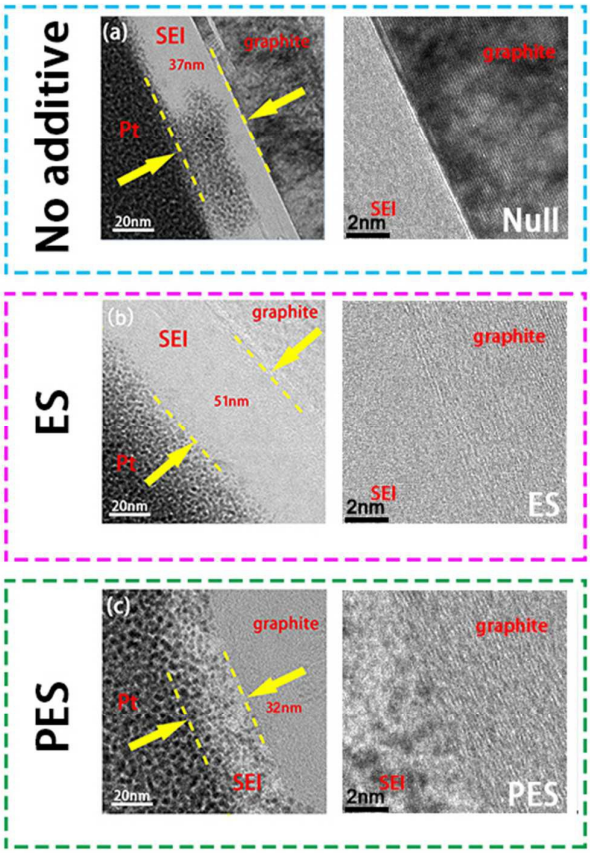

Fig. 5. TEM images of the cross-section of the SEI layers formed (a) without additive, (b) with ES additive, and (c) with PES additive.

signifies the lithium deintercalation process (Fig. S10). During the lithium intercalation process under 0.5 V, the morphology of the surface of HOPG remained unchanged. Further anodic scanning from 1.54 V to 3.00 V of potential caused no change in the SEI layer either (Fig. S10).

Effect of additive on the electrochemical performance

The CV curves measured on coin cells with fresh graphite electrodes and three different electrolytes are shown in Fig. 4a. Note that there are some discrepancies between the CV curves measured in the AFM cell and the coin cell, due to the different graphite materials used in these two measurements (HOPG vs. natural graphite). Different electrode material may affect the potentials for lithium intercalation-deintercalation, but should not affect the potentials for electrolyte reduction. The different IR characteristics of the AFM cell and the coin cell may also cause potential shift in the CV. Still, the comparison indicates that both ES and PES can initiate the cathodic current at higher voltages. The first cathodic peak in the CV curve for the ES-containing cell was at 1.75 V, which agrees well with the CV measured using *in-situ* AFM. The charge-discharge profiles at 0.2 C of the fresh cells are shown in Fig. 4b. For the ES-containing cell, there is a small plateau at 1.75 V (inset in Fig. 4b), indicating the reduction of ES. The initial coulombic efficiencies of the ES-containing cell and PES-containing cell were higher than that of the regular cell without any additives, suggesting that both additives can improve the initial efficiency. However, the capacity of the 2nd discharge is even higher than that of the 1st charge for all three types of cells as shown in Fig. S12, and it appears that there could be an activation process for the graphite electrode.

The effect of the additive on the cycling stability of the cells is demonstrated in Fig. 4c, d and Fig. S14. All coin cells were activated at 0.2 C for two cycles before cycling. At low rates such as 0.2 C and 1 C, the coulombic efficiencies of all three types of cells are close to 100% starting from the 2nd cycle. While tested at 5 C rate, the coulombic efficiency of the ES-containing cell remained mostly 100% during the 100-cycle test. In contrast, the coulombic efficiencies of the regular cell and the PES-containing cell fluctuated significantly below 100% before reaching the 80th cycle, and they increased slowly to approach 100% afterward. The fluctuation in the coulombic efficiency suggests an unstable SEI layer, and electric energy was consumed by decomposition of the electrolyte and irreversible formation of lithium compounds. The SEI layer formed under the presence of ES was very stable and its benefit was especially evident at high rates. Under regular conditions, LIBs will not be charged or discharged at a rate as high as 5 C. The benefit of the ES additive can be critical for protecting the anode from damage in cases when LIBs are accidentally subject to high rate charging or discharging.

Effect of additive on the structure and component of the SEI layer

TEM can further confirm the effect of the additive on the performance of the cell by visualizing the microstructure of the SEI layer, and XPS can help us understand the composition of the SEI layer. For a better comparison, samples of the SEI layer from coin cells after 50 cycles at 5 C rate were analyzed. The TEM images corresponding to the graphite electrodes from the regular cell, the ES-containing cell and the PES-containing cell, respectively, are shown in Fig. 5. In HRTEM observation, we were able to identify the graphite region by the characteristic layered structure, and the Pt region by its dark contrast. The SEI region is defined by its brighter appearance and absence of any crystalline features. The cross-sectional TEM images clearly show that the thickness of the SEI layer was 37nm for the regular cell, 51 nm for the ES-containing cell, and 32nm of the PES-containing cell. More importantly, we can find that the SEI layer in the ES-containing cell was dense without any pores, while the SEI layers of the regular cell and the PES-containing cell contained some black spots, which were pores filled by Pt during Pt deposition (as shown in the high magnification images in Fig. 5). The cross-sectional images confirm that ES can facilitate the formation of a dense SEI layer even at a very high rate, while regular electrolyte or PES additive tends to form a defective SEI layer (Fig. S21). Furthermore, the SEM images show similar observation on the surface morphology of the SEI layers as AFM (Fig. S21). For the SEI layer in the ES-containing cell, the surface of the whole SEI layer is relatively smooth and free of holes. A thick and dense SEI layer can facilitate the desolvation of lithium ions, and remain structurally stable during many charge-discharge cycles. [35] In contrast, the SEI layer formed by the reduction of PES contained many holes. The solvent molecules may easily

Journal of Materials Chemistry A Accepted Manuscript

Please do not adjust margins

View Article Online
DOI: 10.1039/C7TA05469F

Published on 29 August 2017. Downloaded by University Town Library of Shenzhen on 30/08/2017 02:18:08.

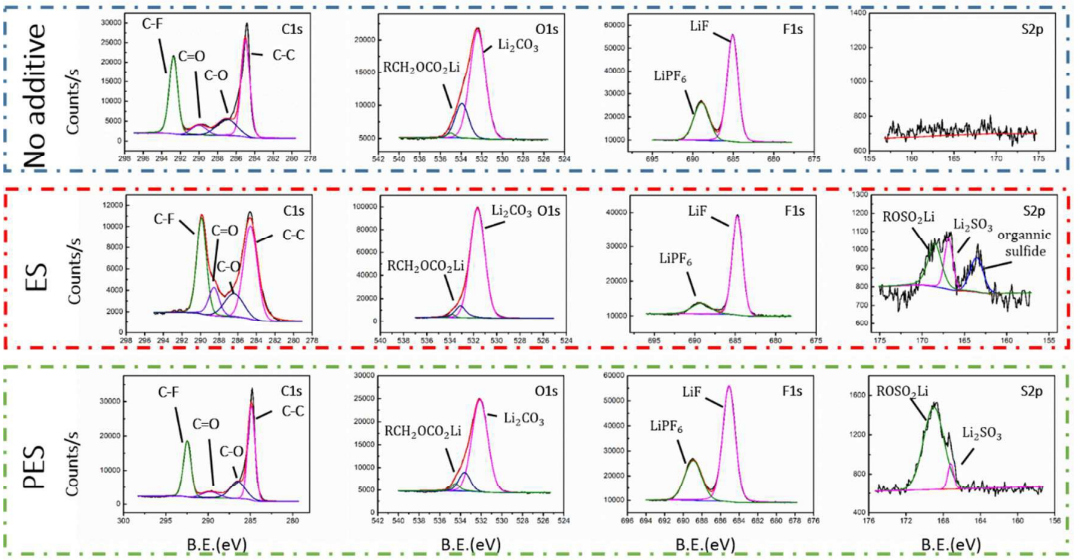

Fig. 6 XPS spectra of the SEI layers formed in regular electrolyte, ES-containing electrolyte, and PES-containing electrolyte.

co-intercalate with Li-ions and can push apart the graphite layers, resulting in the delamination of the SEI layer and the exfoliation of the graphite.[27] The loose structure appeared to be structural unstable and might break easily. The repeated destruction and rebuild of the SEI layer through multiple charging-discharging cycles can lead to decay of the battery performance. Overall, when rapid charging-discharging occurs, SEI layer formed with ES will be more stable than that formed with PES and helps retain the performance of graphite half-cell.

The XPS results of the SEI layers are shown in Fig. 6. The C 1s, O 1s, and F 1s spectra of ES sample and PES sample are quite similar to those of the regular electrolyte. Deconvolution of the high resolution O 1s spectra suggests that the main component of the SEI was $ROCO_2Li$.[6,22, 30, 31] As the S 2p spectra show, ES contributed to the formation of Li_2SO_3, organic sulfides and $ROSO_2Li$[6,32,36,37], indicating that the SEI layer formed by the reduction of ES. In contrast, PES did not generate any noticeable organic sulfides. Both additives generated $ROSO_2Li$ which is not a major component of the SEI, which is reasonable since the concentration of the sulfur-containing additive in the solution was only 1 wt%.[32,36] The SEI layer formed in the regular electrolyte did not contain any sulfur. The XPS result further confirmed that the additives participated in the formation of the SEI layer and they produced sulfur-containing compounds as the first building blocks of the initial SEI layer before the formation of other components derived from the electrolyte.

Conclusions

Using an *in-situ* AFM technology, we can observe the growth history of the SEI layer on a fresh graphite surface in ES-containing and PES-containing electrolytes directly. The results indicated that both ES and PES participated in the formation of the SEI layer but the reduction potential of ES was higher than PES. The effect of the additive on the microstructure and the composition of the SEI layer was analysed using *ex-situ* characterization methods. The results indicate that ES can be reduced to form the initial SEI earlier at a higher potential and it also tends to form a stable and dense SEI layer to protect the surface of graphite electrode. PES as another sulfur-containing additive cannot form an effective SEI layer and the SEI layer can be destructed during multiple charge-discharge cycles, especially at high rates. The *in-situ* AFM observation provided us a vivid image of how the SEI layer gradually formed on a fresh surface of the graphite anode in an LIB during the first cycle, and it clearly verified at what potential the first particles of the SEI started to form.

Acknowledgements

This research was financially supported by the National Materials Genome Project (2016YFB0700600), the Guangdong Innovation Team Project (No. 2013N080), and the Shenzhen Science and Technology Research Grants (Nos. JCYJ20150626110958181, JCYJ20150518092933435).

Notes and references

1. M. Q. Xu, W. S. Li, X. X. Zuo, J. S. Liu and X. Xu, *Journal of Power Sources*, 2007, **174**, 705-710.
2. X. Zuo, M. Xu, W. Li, D. Su and J. Liu, *Electrochemical and Solid-State Letters*, 2006, **9**, A196.

This journal is © The Royal Society of Chemistry 20xx

Journal of Materials Chemistry A Accepted Manuscript

Please do not adjust margins

View Article Online
DOI: 10.1039/C7TA05469F

Published on 29 August 2017. Downloaded by University Town Library of Shenzhen on 30/08/2017 02:18:08.

3. A. M. Haregewoin, A. S. Wotango and B.-J. Hwang, *Energy Environ. Sci.*, 2016, **9**, 1955-1988.
4. K. Xu, *Chem Rev*, 2014, **114**, 11503-11618.
5. G. H. Wrodnigg, J. O. Besenhard and M. Winter, *Journal of The Electrochemical Society*, 1999, **146**, 470-472.
6. A. Li, P. Du, Z. Chen, R. Zhao, W. Huang, L. Zou, D. Huang and H. Chen, *Ionics*, 2015, **21**, 2431-2438.
7. S. Wang, K. Yang, F. Gao, D. Wang and C. Shen, *RSC Adv.*, 2016, **6**, 77105-77110.
8. L. Madec, R. Petibon, K. Tasaki, J. Xia, J. P. Sun, I. G. Hill and J. R. Dahn, *Phys Chem Chem Phys*, 2015, **17**, 27062-27076.
9. B. Li, M. Xu, T. Li, W. Li and S. Hu, *Electrochemistry Communications*, 2012, **17**, 92-95.
10. B. Li, M. Xu, B. Li, Y. Liu, L. Yang, W. Li and S. Hu, *Electrochimica Acta*, 2013, **105**, 1-6.
11. J. Xia, L. Ma, C. P. Aiken, K. J. Nelson, L. P. Chen and J. R. Dahn, *Journal of the Electrochemical Society*, 2014, **161**, A1634-A1641.
12. J. Self, D. S. Hall, L. Madec and J. R. Dahn, *Journal of Power Sources*, 2015, **298**, 369-378.
13. R. R. Liu, X. Deng, X. R. Liu, H. J. Yan, A. M. Cao and D. Wang, *Chem Commun (Camb)*, 2014, **50**, 15756-15759.
14. I. T. Lucas, E. Pollak and R. Kostecki, *Electrochemistry Communications*, 2009, **11**, 2157-2160.
15. Q. P. McAllister, K. E. Strawhecker, C. R. Becker and C. A. Lundgren, *Journal of Power Sources*, 2014, **257**, 380-387.
16. Y. Domi, M. Ochida, S. Tsubouchi, H. Nakagawa, T. Yamanaka, T. Doi, T. Abe and Z. Ogumi, *The Journal of Physical Chemistry C*, 2011, **115**, 25484-25489.
17. D. E. Demirocak and B. Bhushan, *J Colloid Interface Sci*, 2014, **423**, 151-157.
18. X. Deng, X. Liu, H. Yan, D. Wang and L. Wan, *Science China Chemistry*, 2013, **57**, 178-183.
19. X. R. Liu, X. Deng, R. R. Liu, H. J. Yan, Y. G. Guo, D. Wang and L. J. Wan, *ACS Appl Mater Interfaces*, 2014, **6**, 20317-20323.
20. S. Ramdon, B. Bhushan and S. C. Nagpure, *Journal of Power Sources*, 2014, **249**, 373-384.
21. A. v Cresce, S. M. Russell, D. R. Baker, K. J. Gaskell and K. Xu, *Nano Lett*, 2014, **14**, 1405-1412.
22. C. Shen, S. Wang, Y. Jin and W. Q. Han, *ACS Appl Mater Interfaces*, 2015, **7**, 25441-25447.
23. X. R. Liu, L. Wang, L. J. Wan and D. Wang, *ACS Appl Mater Interfaces*, 2015, **7**, 9573-9580.
24. S.-K. Jeong, M. Inaba, Y. Iriyama, T. Abe and Z. Ogumi, *Journal of Power Sources*, 2003, **119-121**, 555-560.
25. J. Zhang, R. Wang, X. Yang, W. Lu, X. Wu, X. Wang, H. Li and L. Chen, *Nano Lett*, 2012, **12**, 2153-2157.
26. J. Zhang, X. Yang, R. Wang, W. Dong, W. Lu, X. Wu, X. Wang, H. Li and L. Chen, *The Journal of Physical Chemistry C*, 2014, **118**, 20756-20762.
27. L. Wang, D. Deng, L. C. Lev and S. Ng, *Journal of Power Sources*, 2014, **265**, 140-148.
28. S. E. Herrera, A. Y. Tesio, R. Clarenc and E. J. Calvo, *Phys Chem Chem Phys*, 2014, **16**, 9925-9929.
29. S.-K. Jeong, M. Inaba, T. Abe and Z. Ogumi, *Journal of The Electrochemical Society*, 2001, **148**, A989.
30. W. Li, A. Xiao, B. L. Lucht, M. C. Smart and B. V. Ratnakumar, *Journal of The Electrochemical Society*, 2008, **155**, A648.
31. A. M. Andersson, D. P. Abraham, R. Haasch, S. MacLaren, J. Liu and K. Amine, *Journal of The Electrochemical Society*, 2002, **149**, A1358.
32. H. Ota, T. Akai, H. Namita, S. Yamaguchi and M. Nomura, *Journal of Power Sources*, 2003, **119-121**, 567-571.
33. C. Ma, Y. Zhao, J. Li, Y. Song, J. Shi, Q. Guo and L. Liu, *Carbon*, 2013, **64**, 553-556.
34. Q.-C. Zhuang, J. Li and L.-L. Tian, *Journal of Power Sources*, 2013, **222**, 177-183.
35. K. Xu, A. von Cresce and U. Lee, *Langmuir*, 2010, **26**, 11538-11543.
36. Xu M, Li W, Lucht B L, *Journal of Power Sources*, 2009, **193**, 804-809.
37. Martin L, Martinez H, Poinot D, *Journal of Power Sources*, 2014, **248**,861-873.

Journal of Materials Chemistry A Accepted Manuscript

Please do not adjust margins